Bestätigung der Metadaten/Metadata Approval Sheet

Sehr geehrte Autoren,
Bitte prüfen Sie diese Angaben sorgfältig. Sie sind für alle nachfolgenden Publikationswege (Print, Online, Abstracting und Indexing, Suchmaschinen etc.) relevant. Änderungen sind später nicht mehr möglich. Bitte führen Sie eventuelle Korrekturen in den beschreibbaren Feldern in der rechten Spalte aus. Bitte bestätigen Sie die Korrektheit der Daten, indem Sie das Feld unten anklicken.

Vielen Dank für Ihre Mitarbeit, De Gruyter

Dear author,
Please check these data carefully. They are relevant for all following publication processes in Abstracting and Indexing Services, search engines. They cannot be changed after publication. Please fill in your corrections within the editable fields in the right column. Please confirm the correct data by clicking the field below.

Thanks for your kind cooperation, De Gruyter

Journal-Name: Zeitschrift für Kristallographie - Crystalline Materials
Article-DOI: 10.1515/zkri-2016-1990

Article-Type:

Article-Title: Crystallographic and computational study of *t*-butyl *N*-[3-hydroxy-1-phenyl-4-(pyridin-2-ylsulfanyl)butan-2-yl]carbamate and its pyrimidin-2-yl analogue

Subtitle:

Author 1:
Surname: Vellasco Junior
First Name: Walcimar T.
Corresponding: no
E-Mail: no
Affiliation: Instituto de Tecnologia em Fármacos – Farmanguinhos, FioCruz –, Fundação Oswaldo Cruz, R. Sizenando Nabuco, 100, Manguinhos, 21041-250 Rio de Janeiro, RJ, Brazil; and Departamento de Química Orgânica, Universidade Federal Fluminense, Instituto de Química, Outeiro de São João Batista, Centro, Niterói, 24020-141, Rio de Janeiro, Brazil

Author 2:
Surname: Gomes
First Name: Claudia R.B.
Corresponding: no

E-Mail: no

Affiliation: Instituto de Tecnologia em Fármacos – Farmanguinhos, FioCruz –, Fundação Oswaldo Cruz, R. Sizenando Nabuco, 100, Manguinhos, 21041-250 Rio de Janeiro, RJ, Brazil

Author 3:

Surname: Vasconcelos

First Name: Thatyana R.A.

Corresponding: no

E-Mail: no

Affiliation: Departamento de Química Orgânica, Universidade Federal Fluminense, Instituto de Química, Outeiro de São João Batista, Centro, Niterói, 24020-141, Rio de Janeiro, Brazil

Author 4:

Surname: Wardell

First Name: James L.

Corresponding: yes

E-Mail: j.wardell@abdn.ac.uk

Affiliation: Instituto de Tecnologia em Fármacos – Farmanguinhos, FioCruz –, Fundação Oswaldo Cruz, R. Sizenando Nabuco, 100, Manguinhos, 21041-250 Rio de Janeiro, RJ, Brazil; and Department of Chemistry, Aberdeen University of Aberdeen, AB 24 3UE, Scotland

Author 5:

Surname: Otero-de-la-Roza

First Name: A. Alberto

Corresponding: no

E-Mail: no

Affiliation: Department of Chemistry, University of British Columbia, Okanagan, 3247 University Way, Kelowna, British Columbia V1V 1V7, Canada

Author 6:

Surname: Jotani

First Name: Mukesh M.

Corresponding: no

E-Mail: no

Affiliation: Department of Physics, Bhavan's Sheth R. A. College of Science, Ahmedabad, Gujarat 380001, India

Author 7:
Surname: Tiekink
First Name: Edward R.T.
Corresponding: yes
E-Mail: edwardt@sunway.edu.my
Affiliation: Research Centre for Chemical Crystallography, Faculty of Science and Technology, Sunway University, 47500 Bandar Sunway, Selangor Darul Ehsan, Malaysia

History Dates:

Received Date: July 17, 2016

Accepted Date: August 23, 2016

Data checked and receipted ☑ **Date:** Sept. 9th, 2016

Wenn Sie die Korrektheit der Daten nicht durch einen Haken bestätigen oder keine Änderungen in diesem Formular angeben, gehen wir davon aus, dass die angegebenen Daten korrekt sind.

If you don't confirm the correctness by checking the box or implement your corrections in this form, we have to presume that all data are correct.

Q1: Please supply first full name of the author A. Otero-de-la-Roza unless this is the name by which the author is commonly known

Walcimar T. Vellasco Junior, Claudia R.B. Gomes, Thatyana R.A. Vasconcelos, James L. Wardell*, A. Otero-de-la-Roza, Mukesh M. Jotani and Edward R.T. Tiekink*

Crystallographic and computational study of *t*-butyl *N*-[3-hydroxy-1-phenyl-4-(pyridin-2-ylsulfanyl)butan-2-yl]carbamate and its pyrimidin-2-yl analogue

DOI 10.1515/zkri-2016-1990
Received July 17, 2016; accepted August 23, 2016

Abstract: The crystal structure analysis of the biologically-relevant title compound (**1**) shows the carbonyl-O2 and amide-H atoms to be anti, and perpendicular relationships between the carbamate residue and the pyridyl ring [dihedral angle = 84.60(10)°] and between the carbamate and aryl ring [74.84(11)°]; the rings are approximately co-planar [12.07(17)°]. An intramolecular hydroxyl-O–H···N(pyridyl) hydrogen bond that closes a S(7) loop is noted. Of interest is the observation that this hydrogen bond is not found in the structure of the pyrimidinyl analogue (**2**) which was characterised as a monohydrate, i.e. **2**·H_2O, in an earlier study. Density-functional theory calculations show the observed conformation in **1** is 2.0 kcal/mol more stable than the conformation where the intramolecular hydrogen bond is absent. This energy difference reduces to ca 0.5 kcal/mol in the case of **2**. The differences in molecular conformations found for **1** and **2** are therefore ascribed to the dictates of overall molecular packing, in particular due to the influence of lattice water in **2**·H_2O.

Keywords: conformation; crystal structure analysis; DFT; 2-Hydroxyethylamine cores; X-ray diffraction.

***Corresponding authors: James L. Wardell,** Instituto de Tecnologia em Fármacos – Farmanguinhos, FioCruz –, Fundação Oswaldo Cruz, R. Sizenando Nabuco, 100, Manguinhos, 21041-250 Rio de Janeiro, RJ, Brazil; and Department of Chemistry, Aberdeen University of Aberdeen, AB 24 3UE, Scotland, E-mail: j.wardell@abdn.ac.uk; and **Edward R.T. Tiekink,** Research Centre for Chemical Crystallography, Faculty of Science and Technology, Sunway University, 47500 Bandar Sunway, Selangor Darul Ehsan, Malaysia, E-mail: edwardt@sunway.edu.my
Walcimar T. Vellasco Junior: Instituto de Tecnologia em Fármacos – Farmanguinhos, FioCruz –, Fundação Oswaldo Cruz, R. Sizenando Nabuco, 100, Manguinhos, 21041-250 Rio de Janeiro, RJ, Brazil; and Departamento de Química Orgânica, Universidade Federal Fluminense, Instituto de Química, Outeiro de São João Batista, Centro, Niterói, 24020-141, Rio de Janeiro, Brazil
Claudia R.B. Gomes: Instituto de Tecnologia em Fármacos – Farmanguinhos, FioCruz –, Fundação Oswaldo Cruz, R. Sizenando Nabuco, 100, Manguinhos, 21041-250 Rio de Janeiro, RJ, Brazil
Thatyana R.A. Vasconcelos: Departamento de Química Orgânica, Universidade Federal Fluminense, Instituto de Química, Outeiro de São João Batista, Centro, Niterói, 24020-141, Rio de Janeiro, Brazil
A. Otero-de-la-Roza: Department of Chemistry, University of British Columbia, Okanagan, 3247 University Way, Kelowna, British Columbia V1V 1V7, Canada
Mukesh M. Jotani: Department of Physics, Bhavan's Sheth R. A. College of Science, Ahmedabad, Gujarat 380001, India

Introduction

Compounds having 2-hydroxyethylamine cores have useful biological activities as aspartyl protease enzymes inhibitors, [1, 2], as inhibitors of BACE-1 to combat Alzheimer's disease [3], as anti-malarial agents [4–8], as anti-bacterial agents [7], and in the treatment of leishmaniasis/HIV-1 co-infections [9]. In continuation of our structural studies on these and related compounds [10, 11], herein the crystal structure of the title compound, **1** (Figure 1) is described.

During the analysis of the molecular structure of **1** it was apparent that an intramolecular hydroxyl-O–H···N(pyridyl) hydrogen bond had formed. This was unexpected as in the previously reported pyrimidin-2-yl analogue, **2**, isolated as a monohydrate, no such hydrogen bond was formed [10]. While the absence of an intramolecular hydroxyl-O–H…N(pyrimidinyl) hydrogen bond in **2** might be related to the influence of a solvent molecule of water incorporated in the crystal lattice, the different behaviour was not anticipated as both compounds were prepared and recrystallised under very similar conditions [10]. Accordingly, it was thought of interest to complement the X-ray structural studies with quantum chemical calculations in order to understand the different crystallisation outcomes/molecular conformations. The results of this investigation are reported herein.

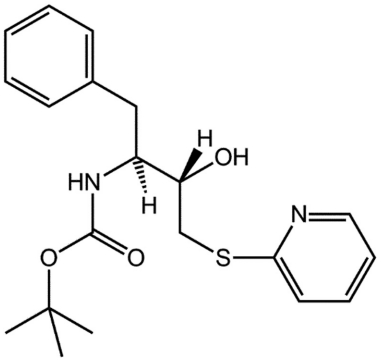

Fig. 1: Chemical structure of **1**: *tert*-butyl *N*-[3-hydroxy-1-phenyl-4-(pyridin-2-ylsulfanyl)butan-2-yl]carbamate.

Experimental

Synthesis and characterisation

A solution of 2-mercaptopyridine (1.5 mmol), (2*S*,2*S*)-boc-phenylalanine epoxide (1.6 mmol) and triethylamine (1.6 mmol) in methanol (10 mL) was stirred at room temperature for 2 h. The reaction mixture was rotary evaporated. The solution was concentrated in vacuo and to the residue was added 5% aqueous HCl solution. The mixture was extracted with dichloromethane and the combined organic layers were washed with brine, dried over anhydrous Na_2SO_4 and evaporated, giving **1** in 98% yield. The crude product was crystallised from methanol/water (7:3), m.pt: 372–373 K. The sample used in the structure determination was grown from its EtOH solution.

^{1}H-NMR (DMSO-d$_6$): 8.39 (d, 1H, J = 4.2, H5′); 7.62 (dt, 1H, ^1J = 8.0, ^2J = 1.8, H3′); 7.29 (d, 1H, J = 9.5, H2′); 7.25-7.22 (m, 2H, Ph); 7.18-7.14 (m, 3H, Ph); 7.09 (ddd, 1H, ^1J = 7.3, ^2J = 5.0, ^3J = 0.7, H4′); 6.70 (d, 1H, J = 8.8, NH); 5.37 (d, 1H, J = 5.8, OH); 3.66–3.58 (m, 2H, H3 and H2); 3.51 (dd, 1H, ^1J = 13.5, ^2J = 3.4, Hb); 3.08-3.01 (m, 2H, H1a and H4b); 2.57 (dd, 1H, ^1J = 13.7, ^2J = 10.2, H4a); 1.26 (s, 9H, Boc).

^{13}C-NMR (DMSO-d$_6$): 158.7; 155.2; 149.1; 139.5; 136.5; 129.1; 127.8; 125.6; 121.7; 119.5; 77.4; 72.4; 56.2; 35.6; 34.1; 28.1.

EM-ESI (m/z): 397.2 (M^++Na, 100%).

IR ν_{max} (KBr pellets, cm^{-1}): 3356 (OH); 1686 (C=O); 2979 (NH); 1578 (C=C and C=N); 659 (C–S).

Crystal structure determination

Intensity data were measured at 100 K on a Rigaku Saturn724+ CCD with Mo Kα radiation. Data processing and absorption correction were accomplished with CrystalClear-SM Expert [12]. With the use of SHELXS-97 [13] and SHELXL-2014/7 [14] programs integrated into WinGX [15], the structure was solved by direct methods and refined on F^2 by full-matrix least-squares with anisotropic displacement parameters for all non-hydrogen atoms. The C-bound H atoms were placed on stereochemical grounds and refined in the riding model approximation with U_{iso} = 1.2–1.5U_{eq}(carrier atom). The O- and N-bound H atoms were refined with O–H = 0.84 ± 0.01 and N–H = 0.88 ± 0.01 Å, respectively, and with U_{iso} = 1.5U_{eq}(O) and U_{iso} = 1.2U_{eq}(N). A weighting scheme of the form $w = 1/[\sigma^2(F_o^2) + (0.034P)^2 + 0.034P]$ where $P = (F_o^2 + 2F_c^2)/3$ was introduced. The absolute structure was determined based on 1202 Friedel pairs included in the data set, and confirmed that expected from the synthesis. Unit cell data, X-ray data collection parameters, and details of the structure refinement are given in Table 1. The programs ORTEP-3 for Windows [15], PLATON [16], QMol [17] and DIAMOND [18] were also used in the analysis.

Computational chemistry

Density-functional theory (DFT) calculations were performed using the Gaussian09 software package [19]. The LC-wPBE [20, 21] exchange-correlation functional was coupled with the exchange-hole dipole moment (XDM) dispersion model [22, 23] as implemented in the postg program [24]. The 6-31+G* basis set was employed as was Gaussian's ultrafine setting for the numerical integration grid.

The pyridyl and pyrimidinyl derivatives, **1** and **2**, were subjected to full geometry relaxation. At the minimum-energy structures, the dihedral angle along the C–S bond was rotated, and geometry relaxations at fixed values for that angle were conducted in order

Table 1: Crystallographic data and refinement details for **1**.[a]

Formula	$C_{20}H_{26}N_2O_3S$
Formula weight	374.49
Crystal colour, habit	Colourless needle
Crystal size/mm	0.04 × 0.07 × 0.65
Crystal system	Monoclinic
Space group	$P2_1$
a/Å	10.2898(8)
b/Å	9.8137(7)
c/Å	10.4918(8)
β/°	112.340(8)
V/Å^3	979.95(14)
Z/Z'	2/1
D_c/g cm^{-3}	1.269
F(000)	400
μ(Mo$K\alpha$)/mm^{-1}	0.187
Measured data	7268
θ range/°	3.1–27.5
Unique data	3905
R_{int}	0.045
Observed data ($I \geq 2.0\sigma(I)$)	3460
R, obs. data; all data	0.040; 0.046
R_w, obs. data; all data	0.087; 0.090

[a]Supplementary material: Crystallographic data (excluding structure factors) for the structures reported in this paper have been deposited with the Cambridge Crystallographic Data Centre as supplementary publication no. CCDC-1493079. Copies of available material can be obtained free of charge, on application to CCDC, 12 Union Road, Cambridge CB2 1EZ, UK, (fax: +44-(0)1223-336033 or e-mail: deposit@ccdc.cam.ac.uk). The list of Fo/Fc-data is available from the author up to 1 year after the publication has appeared.

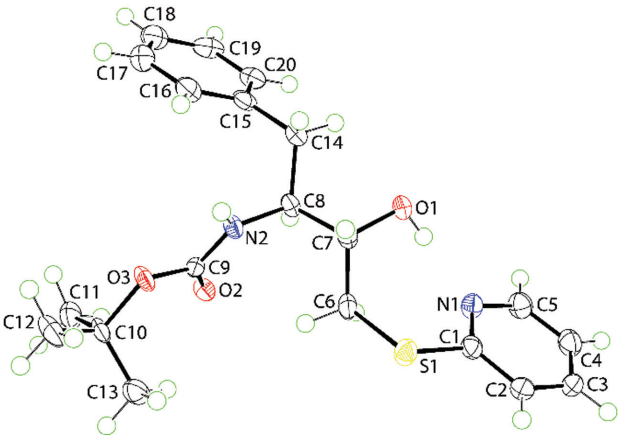

Fig. 2: Molecular structure of **1** showing the atom labelling scheme. The diagram is drawn at the 70% probability level.

to examine the energy profile with respect to rotation around the C–S bond.

Hirshfeld surface analysis

Crystal Explorer 3.1 [25] was employed to generate Hirshfeld surfaces mapped over $d_{norm,}$ shape-index, curvedness and electrostatic potential for each of **1** and **2**·H_2O. The electrostatic potentials were calculated using TONTO [26, 27] which was integrated into *Crystal Explorer*. The electrostatic potentials were mapped on Hirshfeld surfaces using the STO-3G basis set at the Hartree-Fock level of theory over the range ±0.08 and ±0.13 au for **1** and **2**·H_2O, respectively. The contact distances d_i and d_e from the Hirshfeld surface to the nearest atom inside and outside, respectively, enables the analysis of the intermolecular interactions through the mapping of d_{norm}. Finally, the combination of d_e and d_i in the form of two-dimensional fingerprint plots [28] provides a convenient summary of intermolecular contacts in the respective crystal.

Results and discussion

Crystal and molecular structures

The molecular structure of **1** is shown in Figure 2. Each of the C7 and C8 stereocentres has an *S*-configuration as expected from the synthetic protocols. The four atoms comprising the carbamate moiety are strictly co-planar (r.m.s. deviation = 0.0004 Å) and the carbonyl-O2 and amide-H atoms are anti. The dihedral angle between the carbamate and the pyridyl ring is 84.60(10)°, indicating an almost perpendicular relationship. The comparable angle formed with the aryl ring is 74.84(11)°, and the angle between the two rings is 12.07(17)°. From the torsion angle data collated in Table 2, it is evident that there is an extended approximately planar C_4S chain running through the molecule, i.e. the S1–C6–C7–C8 torsion angle is –168.42(19)° and C6–C7–C8–C14 is –172.7(2)°. In this description, the hydroxyl and 2-pyridyl groups lie to one side, and the carbamate ester to the other. Finally, the O1–C7–C8–N2 torsion angle of –169.8(2)°, where the terminal atoms are anti, indicates co-planarity in this residue. The hydroxyl group is in an orientation to allow the formation of an intramolecular hydroxyl-O–H···N(pyridyl) hydrogen bond that closes a S(7) loop, Table 2.

The most prominent feature of the molecular packing is the formation of amide-N–H…O(carbonyl) hydrogen bonds, Table 3, made possible by the anti relationship between the amide-H and carbonyl-O atoms. The result is the formation of helical supramolecular helical chains along the *b*-axis, Figure 3a. Chains are assembled into layers in the *ab*-plane by π(pyridyl)…π(aryl) interactions operating in the *a*-direction, Table 3 and Figure 3b. The

Table 2: Selected torsion angle data (°) in the experimental (**1** and **2**·H_2O [10]) and geometry-optimised structures of **1** and **2**.[a]

Torsion angle	Experimental 1	Geometry optimised 1	Experimental 2·H_2O	Geometry optimised 2
	Y = C2	Y = C2	Y = N3 (pym)	Y = N3 (pym)
S1–C6–C7–O1	68.4(3)	88.9	65.2(3)	88.9
C6–S1–C1–N1	14.2(3)	16.7	178.6(2)	5.7
C6–S1–C1–Y	–167.2(2)	–163.9	–0.9(3)	–173.7
C1–S1–C6–C7	–88.1(2)	–79.2	89.9(2)	–75.1
S1–C6–C7–C8	–168.42(19)	–151.9	–176.4(2)	–151.9
O1–C7–C8–N2	–169.8(2)	–173.2	–179.3(3)	–176.2
O1–C7–C8–C14	–48.0(3)	–49.6	–57.7(3)	–52.9
N2–C8–C14–C15	–58.6(3)	–53.6	–70.4(3)	–50.8
N2–C8–C7–C6	65.5(3)	64.4	62.0(3)	61.2
C6–C7–C8–C14	–172.7(2)	–172.1	–176.3(3)	–175.6
C8–N2–C9–O2	–0.1(4)	20.5	–3.5(5)	26.0
C8–N2–C9–O3	180.0(2)	–161.0	–165.2(3)	–155.2

[a]Refer to Figure 2 for the numbering scheme.

Table 3: Summary of intermolecular interactions (A–H…B; Å, °) operating in the crystal structure of **1**.[a]

A	H	B	A–H	H…B	A…B	A–H…B	Symmetry operation
O1	H1o	N1	0.85(3)	1.94(3)	2.782(3)	173(3)	*x*, *y*, *z*
N2	H2n	O2	0.871(14)	2.181(15)	3.029(4)	164(3)	2 − *x*, ½ + *y*, −*z*
Cg(N1,C1–C5)		Cg(C15–C20)			3.6868(18)	12.07(14)	−1 + *x*, *y*, *z*

[a]Cg corresponds to the ring centroid of the specified atoms.

layers stack along the *c*-axis without specific interactions between them, Figure 3c.

Computational chemistry

The key observation differentiating the molecular structures of **1** and **2** is that in the former, an intramolecular hydrogen bond is formed but, in the latter, despite having two nitrogen atom acceptors, the hydrogen bond of **1** is not replicated in the experimental structure of **2**·H_2O. As seen in the overlay diagram of the experimental structures, Figure 4a, the lack of this hydrogen bond arises as a result of a very different orientation of the 2-pyrimidinyl ring in **2**·H_2O cf. the 2-pyridyl ring in **1**.

The molecular structure **1** was subjected to unconstrained geometry-optimisation calculations and an illustration of the overlap between energy-minimised structure and experimental (crystallographic) structure is shown in Figure 4b. From this, it is apparent that while some differences exist, there is a high degree of agreement between the molecular structures. From the torsion angle data in Table 2, the major differences relate to twists about the S1–C6, C6–C7 and N2–C9 bonds; other differences are usually <5°. There are also differences in the relative orientations of the terminal rings so while they were approximately co-planar in experimental **1**, i.e. the dihedral angle = 12.07(17)°, they are twisted in geometry-optimised **1**, i.e. that dihedral angle is 65.1°. The most notable feature of the optimised structure is the persistence of the intramolecular hydroxyl-O–H···N(pyridyl) hydrogen bond.

The experimental structure of **2**, sans the water molecule of crystallisation, was also subjected to geometry-optimisation calculations. The overlay diagram of experimental **2** and geometry-optimised **2**, Figure 4c, and the data in Table 2, suggest perturbations in the molecular geometries, with changes in torsion and, crucially, evidence for intramolecular hydroxyl-O–H···N(pyrimidinyl) hydrogen bond formation was found.

When the optimised forms of **1** and **2** are overlapped, Figure 4d, the agreement between the structures is closer than shown in Figure. 4a, with the obvious similarity not found in the experimental structures, being in the S-terminus whereby the 2-pyridyl ring in **1** is syn to the hydroxyl group similar to the 2-pyrimidinyl group in **2**. Based on these results, there appear to be distinct conformational preferences in **1** and **2** and in order to test this further, additional calculations were performed.

For each compound, a potential energy (PE) profile was constructed by rotating about the C6–S1 bond and fixing the value of the dihedral angle but allowing the residues on either side of the bond to relax. The PE profiles of the two compounds, Figure 5, indicate that the initial conformer of each compound was the minimum energy structure and rotation of the defined torsion leads to the less stable conformers. This was particularly the case for **2** where the energy differences between the most stable conformation and the one with no hydrogen bond as smaller, i.e. 0.5 kcal/mol compared with the differences calculated for **1**, i.e. >2.0 kcal/mol. Therefore, it is likely that the differences in molecular conformations are related to the influence of molecular packing, in particular the role of lattice water in **2**·H_2O. A deeper analysis of the molecular packing is given *Hirshfeld surface analysis*.

Hirshfeld surface analysis of 1 and 2.H_2O

In this section an analysis of the molecular packing in **1** based on Hirshfeld surface analysis will be contrasted to that in **2**·H_2O. While the molecular packing for **1** has been described above, it is salient to recall the essential features of the molecular packing for **2**·H_2O here [10] before describing the Hirshfeld surface analyses for **1** and **2**·H_2O.

In the crystal of **2**·H_2O, linear supramolecular chains mediated by amide-N–H…O(carbonyl) hydrogen bonds are found, Figure 6. Two chains are linked into a tape via hydrogen bonding involving the water molecule of crystallisation. The water molecule forms three significant interactions, accepting a hydrogen from a hydroxyl group, and donating hydrogen atoms to a symmetry related hydroxyl group and to a pyrimidinyl-nitrogen atom.

The comparison of Hirshfeld surfaces computed for **1** and its pyrimidin-2-yl analogue, **2**·H_2O, i.e. containing a lattice water molecule, successfully explains the influence of the latter in the crystal. The Hirshfeld surfaces mapped

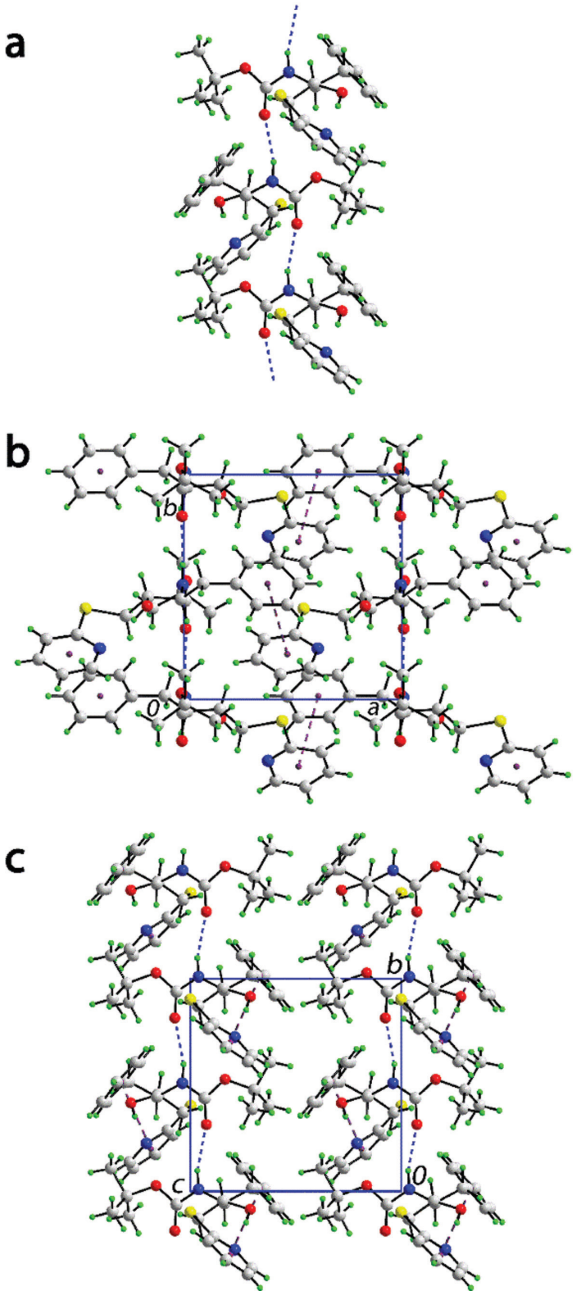

Fig. 3: Molecular packing in **1**: (a) a supramolecular helical chain along the *b*-axis moderated by amide-N–H…O(carbonyl) hydrogen bonds, shown as blue dashed lines, (b) supramolecular layer in the *ab*-plane whereby the chains of (a) are connected by π(pyridyl)…π(aryl) interactions, shown as purple dashed lines, and (c) a view of the unit cell contents shown in projection down the *a*-axis, highlighting the stacking of layers along *c*.

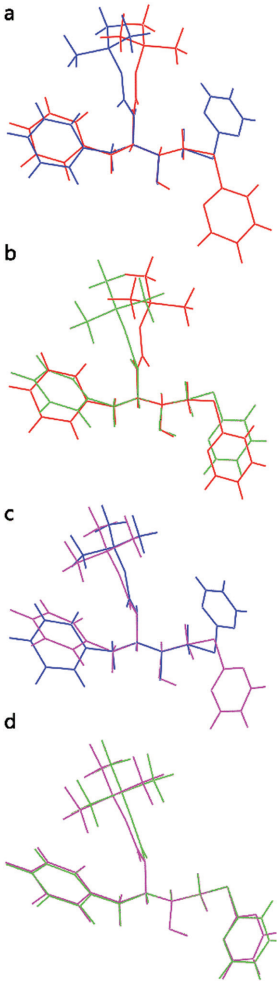

Fig. 4: Overlay diagrams of the molecular structures in **1** and **2**, whereby the C6–C7–C8 chains have been made coincident: (a) experimental **1** (red image) and experimental **2** in **2**·H_2O (blue), (b) experimental **1** (red image) and geometry optimised **1** (green), (c) experimental **2** in **2**·H_2O (blue image) and geometry optimised **2** (purple), and (d) geometry-optimised **1** (green image) and geometry-optimised **2** (purple).

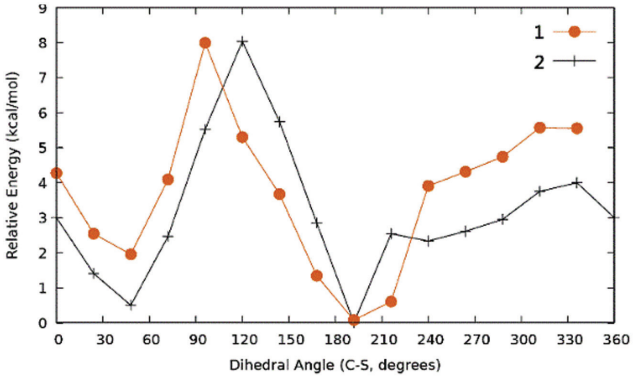

Fig. 5: Potential energy curves for **1** and **2**, whereby rotation about the C6–S1 bond in 20° increments were effected.

over $d_{norm,}$ d_e, shape-index, curvedness and electrostatic potential clearly indicate the formation of different supramolecular assemblies through the different intermolecular interaction profiles for molecules **1** and **2**·H_2O in their respective crystal. Thus, the shape of surfaces, the number

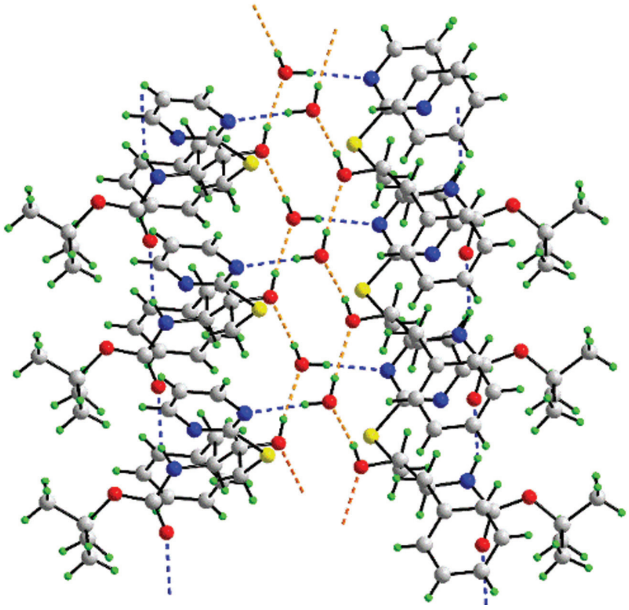

Fig. 6: Molecular packing in **2**·H_2O: supramolecular tape moderated by amide-N–H…O(carbonyl) hydrogen bonds, highlighting the pivotal role of water molecules forming water-O–H···N(pyrimidinyl), water-O–H···O(hydroxyl) and hydroxyl-O–H···O(water) hydrogen bonds. The N–H···O and O–H···O hydrogen bonds are shown as blue and orange dashed lines, respectively.

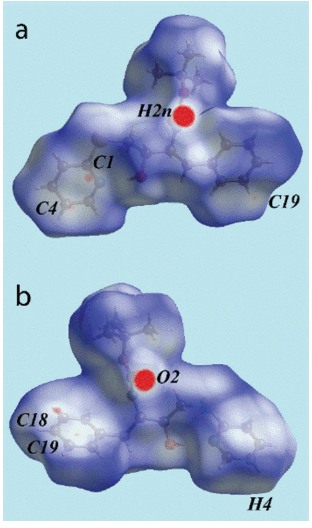

Fig. 7: Two views of Hirshfeld surfaces mapped over d_{norm} for **1**, where the atom labels near red spots indicate the intermolecular interactions.

of bright-red spots on the d_{norm} mapped surfaces and the red and blue regions on the Hirshfeld surfaces mapped over electrostatic potential are different for **1** and **2**.

In the two views of the Hirshfeld surface mapped over d_{norm} in the range −0.12 to 1.4 Å for **1** are shown in Figure 7.

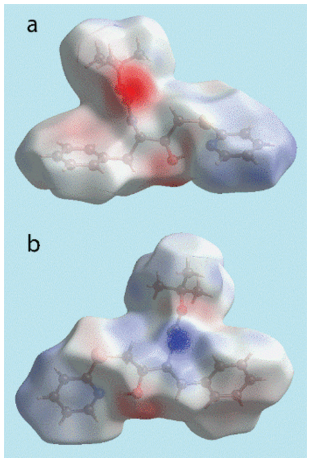

Fig. 8: Two views of the Hirshfeld surface mapped over electrostatic potential for **1**. The red and blue regions represent negative and positive electrostatic potentials, respectively.

The bright-red spots appearing near the amide-H2n and carbonyl-O2 atoms indicate their roles as the respective donor and acceptor in the dominant N–H···O hydrogen bonding; these also appear as blue and red regions corresponding to positive and negative electrostatic potentials on the Hirshfeld surface mapped over electrostatic potential in Figure 8. The presence of a short intermolecular C···C contacts between the pairs of pyridyl and aryl carbons, C1, C18 and C4, C19, Table 4, indicative of π···π contacts, Table 3, are also viewed as light-red spots near these atoms in Figure 7. In addition, a pair of faint-red spots near benzene-C19 and pyridyl-H4 also indicate the presence of short intermolecular C···H/H···C contacts, Table 4.

Table 4: Additional short interatomic contacts (Å) in **1** and **2**·H_2O.

Contact	Distance (Å)	Symmetry operation
1		
C1…C18	3.336(5)	−1 + *x*, *y*, *z*
C4…C19	3.367(4)	−1 + *x*, *y*, *z*
C19…H4	2.73	2 − *x*, ½ + *y*, 1 − *z*
O1…H13B	2.62	*x*, *y*, 1 + *z*
O1…H12C	2.67	2 − *x*, ½ + *y*, −*z*
O2…H16	2.69	2 − *x*, ½ + *y*, −*z*
H1o…H12C	2.38	2 − *x*, ½ + *y*, −*z*
H13A…H14A	2.24	2 − *x*, ½ + *y*, −*z*
2·H_2O		
O2…H19	2.66	*x*, −1 + *y*, *z*
N1…H6	2.63	½-*x*, −½+*y*, 2 − *z*
H1…H26	2.39(3)	*x*, 1 + *y*, *z*
H10…H24	2.36	−½ + *x*, ½ + *y*, *z*
H12…H14	2.33	*x*, −1 + *y*, *z*

In the Hirshfeld surface mapped over d_{norm} for the lattice water-containing pyrimidin-2-yl analogue, **2**·H_2O, Figure 9, the increase in the number of dominating intermolecular interactions is viewed as a greater number of bright-red spots appearing on the surface near the O1w, H1w, H3n, O2, H1o and N1 atoms. The hydrogen bond involving the hydroxyl-O1 and water-H2w are inside the surface and shown with dashed lines between them in Figure 9. The respective donors and acceptors of hydrogen bonds in this molecule are also viewed as blue and red regions on the Hirshfeld surface mapped over electrostatic potential in Figure 10.

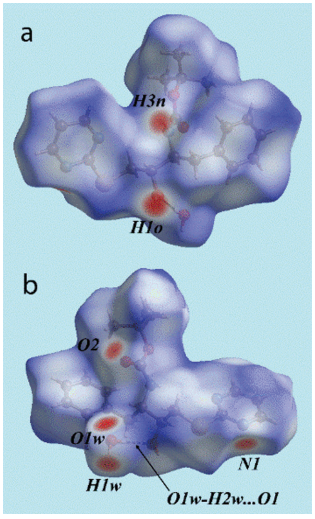

Fig. 9: Two views of Hirshfeld surfaces mapped over d_{norm} for **2**·H_2O, where the atom labels near red spots indicate the intermolecular interactions.

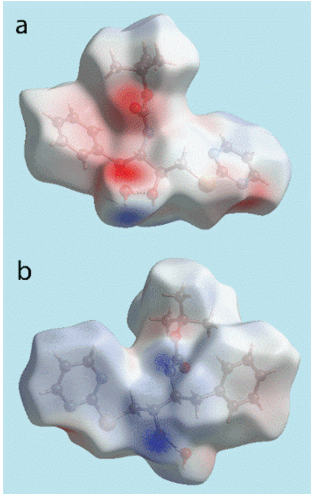

Fig. 10: Two views of the Hirshfeld surface mapped over electrostatic potential for **2**·H_2O. The red and blue regions represent negative and positive electrostatic potentials, respectively.

The overall two-dimensional fingerprint plots corresponding to different percentage contributions from various non-bonded contacts for **1** and **2**·H_2O are illustrated in Figure 11; and are summarised quantitatively in Table 5. The fingerprint plots delineated into H···H, O···H/H···O, C···H/H···C and S···H/H···S contacts [29] are shown in Figures 11b–e, respectively. In addition, the plots delineated into C···C contacts for **1** and N···H/H···N for **2**·H_2O are included in Figure 11f due to their significance in their respective crystal structures.

The fingerprint plots delineated into H···H contacts for **1** and **2**·H_2O, Figure 11b, show the points to be distributed in different patterns with respect to their molecular conformation and have their respective peaks at $d_e = d_i \sim 1.1$ Å for **1**, and 1.2 Å for **2**·H_2O corresponding to short interatomic H···H contacts, Table 4. The decrease in the percentage contribution from H···H contacts to the Hirshfeld surface of **2**·H_2O is due to the presence of O–H···O, O–H···N and N–H···O hydrogen bonding involving the solvent water molecule. The absence of such hydrogen bonding interactions in **1** enables more hydrogen atoms on the surface to form intermolecular interactions. An almost the same percentage contribution from O···H/H···O contacts to the Hirshfeld surfaces is noted for **1** and **2**·H_2O, Figure 11c, Table 4, although these arise from different intermolecular contacts, i.e. the short interatomic O···H/H···O contacts for the former and the dominating hydrogen bonds involving water in the latter. A pair of spikes with the tip at $d_e + d_i \sim 2.2$ Å in the fingerprint plot of **1** arises from intermolecular N–H···O interaction whereas in the respective plot for **2**·H_2O the tip at $d_e + d_i \sim 2.0$ Å derives from O–H···O interactions masking the intermolecular N–H···O interactions.

In the absence of C–H···π interactions in the crystal and the characteristic wings in the fingerprint plot delineated into C···H/H···C contacts, Figure 11d, the forceps-like end at $d_e + d_i \sim 2.7$ Å with 11.5% contribution to the surface for **1** is the result of short interatomic contacts, Table 4. The 14.3% contribution from these contacts in **2**·H_2O are a result of the different distribution of points in the plot at (d_e, d_i) distances greater than van der Waals separations, hence do not have their influence on the crystal packing. Finally, the 4.6 and 5.0% contributions from S···H/H···S contacts to the Hirshfeld surfaces for **1** and **2**·H_2O, Figure 11e, showing an asymmetric distribution of points with the tips at distances greater than van der Waals distances indicate these do not have a significant influence on the molecular packing.

The 8.1% contribution from N···H/H···N contacts to the Hirshfeld surface of **2**·H_2O is the result of O–H···N hydrogen bonding involving the solvent water molecule,

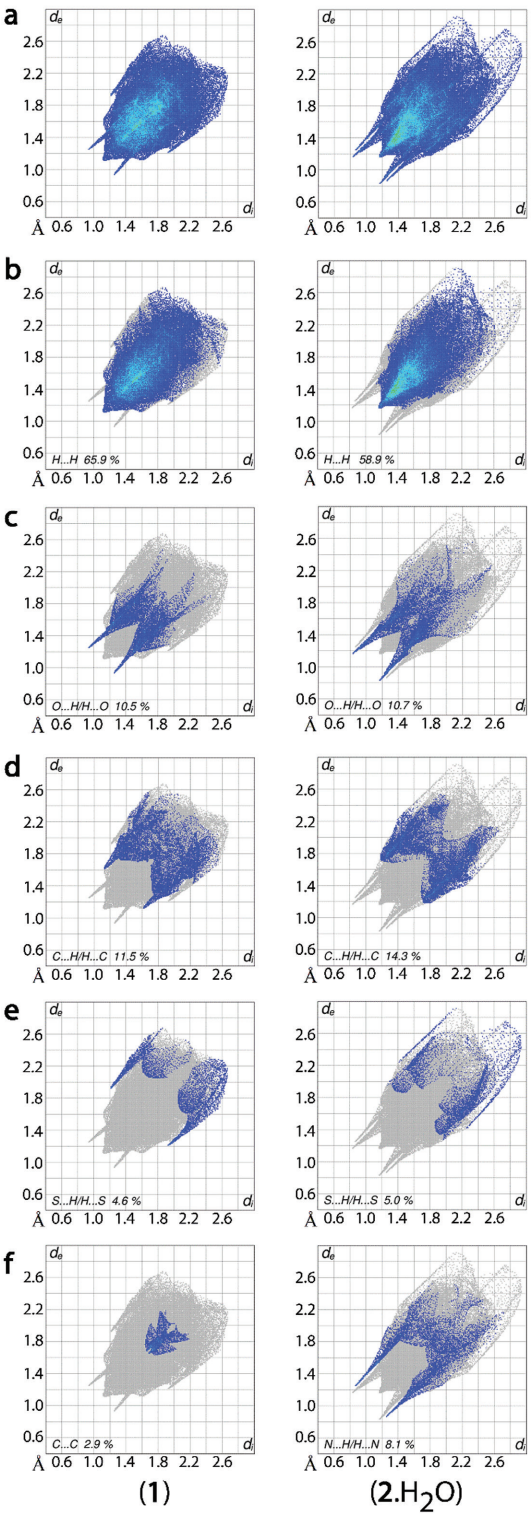

Fig. 11: Two-dimensional fingerprint plots: (a) full, and delineated into (b) H···H, (c) O···H/H···O, (d) C···H/H···C, (e) S···H/H···S, and (f) C···C for **1** and N···H/H···N for **2**·H_2O interactions.

and is viewed as a pair of spikes in the outer part of the plot at $d_e + d_i \sim 2.1$ Å, Figure 11f; a very small percentage contribution, i.e. 1.5%, from these contacts in the structure

Table 5: Percentage contributions of various intermolecular contacts to the Hirshfeld surface areas of **1** and **2**·H_2O.

Contact	% contribution	
	1	**2·H_2O**
H···H	65.9	58.9
O···H/H···O	10.5	10.7
C···H/H···C	11.5	14.3
S···H/H···S	4.6	5.0
N···H/H···N	1.5	8.1
C···C	2.9	0.1
C···S/S···C	2.4	0.4
N···S/S···N	0.5	0.3
S···O/O···S	0.0	1.0
C···N/N···C	0.1	0.0
S···S	0.0	0.5
C···O/O···C	0.1	0.2

of **1** clearly indicates the absence of such interactions. The C···C contacts are assigned to short interatomic C1···C18 and C4···C19 contacts listed in Table 4 and π···π stacking interactions between symmetry related pyridyl and aryl rings as described in the earlier discussion of the molecular packing for **1** appear as the distinct distribution of points in the plot delineated into C···C contacts, Figure 11f. A pair of small tips at $d_e + d_i \sim 3.3$ Å belong to the C1···C18 contact whereas the points distributed around these tips correspond to other C···C contacts, and the points around $d_e = d_i \sim 1.9$ Å result from π···π contacts. The presence of π···π stacking interactions is also indicated through the appearance of red and blue triangle pairs on the Hirshfeld surface mapped with shape-index property identified with arrows in the image of Figure 12a, and in the flat

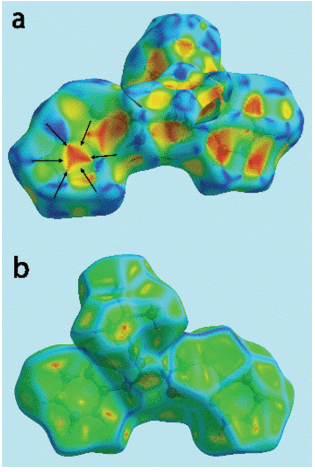

Fig. 12: A view of Hirshfeld surface for **1** mapped over (a) shape-index and (b) curvedness.

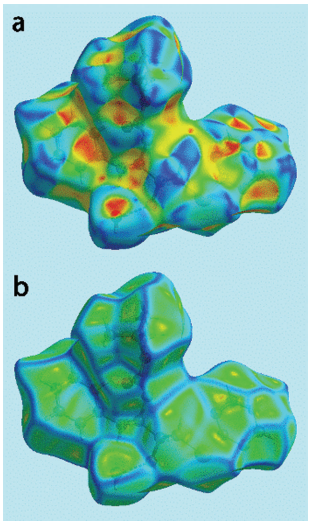

Fig. 13: A view of Hirshfeld surface for **2**·H_2O mapped over (a) shape-index and (b) curvedness.

region on the Hirshfeld surface mapped over curvedness in Figure 12b.

In the structure of **2**·H_2O, the orientation of aryl and pyrimidinyl rings around the C_5S backbone prevents them from forming such contacts resulting in a negligible contribution to the surface. The images corresponding to Hirshfeld surface mapped with shape-index property and curvedness in Figures 13a and b are consistent with this conclusion.

Conclusions

The experimental molecular structures of **1** and **2** in **2**·H_2O, determined on crystals prepared under essentially the same conditions, present two different conformations with the former featuring an intramolecular hydroxyl-O–H···N(pyridyl) hydrogen bond which density-functional calculations suggest is ca 2.0 kcal/mol more stable that the conformation where this hydrogen bond is absent. In the case of **2**·H_2O, the putative conformation where the hydrogen bond is present is only 0.5 kcal/mol more stable that the conformation where the hydrogen bond is absent. Under these circumstances, the energy gain from global crystal packing, most notably the involvement of lattice water, more than compensates the adoption of the high-energy molecular conformation found in the structure of **2**·H_2O.

Acknowledgments: The use of the EPSRC X-ray crystallographic service at the University of Southampton, England, and the valuable assistance of the staff there is gratefully acknowledged. JLW also acknowledges support from CAPES (Brazil). AOR thanks the Spanish Malta/Consolider initiative (no. CSD2007-00045).

References

[1] A. Brik, C.-H. Wong, *Org. Biomol. Chem.* **2003**, *1*, 5.
[2] A. K. Ghosh, G. Bilcer, G. Schiltz, *Synthesis* **2001**, 2203.
[3] L. R. Marcin, M. A. Higgins, F. C. Zusi, Y. Zhang, M. F. Dee, M. F. Parker, J. K. Muckelbauer, D. M. Camac, P. E. Morin, V. Ramamurthy, A. J. Tebben, K. A. Lentz, J.E. Grace, J. A. Marcinkeviciene, L. M. Kopcho, C. R. Burton, D. M. Barten, J. H. Toyn, J. E. Meredith, C. F. Albright, J. J. Bronson, J. E. Macor, L. A. Thompson, *Bioorg. Med. Chem.Lett.* **2011**, *21*, 537.
[4] W. Cunico, M. L. G. Ferreira, T. G. Ferreira, C. Penido, M. G. M. O. Henriques, L. G. Krettli, F. P. Varotti, A. U. Krettli, *Lett. Drug Des. Discov.* **2008**, *5*, 178.
[5] W. Cunico, C. R. B. Gomes, M. Moreth, D. P. Manhanini, I. H. Figueiredo, C. Penido, M. G. M. O. Henriques, F. P. Varotti, A. U. Krettli, *Eur. J. Med. Chem.* **2009**, *44*, 1363.
[6] W. Cunico, C. R. B. Gomes, V. Facchinetti, M. Moreth, C. Penido, M. G. M. O. Henriques, F. P. Varotti, L. G. Krettli, A. U. Krettli, F. S. da Silva, E. R. Caffarena, C. S. de Magalhães, *Eur. J. Med. Chem.* **2009**, *44*, 3816.
[7] W. Cunico, C. R. B. Gomes, M. L. G. Ferreira, T. G. Ferreira, D. Cardinot, M. V. N. de Souza, M. C. S. Lourenço, *Eur. J. Med. Chem.* **2011**, *46*, 974.
[8] W. T. Vellasco Junior, G. P. Guedes, T. R. A. Vasconcelos, M. G. F. Vaz,; M. V. N. Souza, A. U. Krettli, L. G. Krettli, A. C. C. Aguiar, C. R. B. Gomes, W. Cunico, *Eur. J. Med. Chem.* **2011**, *46*, 5688.
[9] N. Trudel, R. Garg, N. Messier, S. Sundar, M. Ouellette, M. J. Tremblay. *J. Infect. Dis.* **2008**, *198*, 1292.
[10] C. R. B. Gomes, T. R. A. Vasconcelos, W. T. Vellasco Junior, J. L.Wardell, S. M. S. V. Wardell, and E. R. T. Tiekink, *Acta Cryst. E* **2011**, *67*, o2313.
[11] C. R. B. Gomes, T. R. A. Vasconcelos, W. T. Vellasco Junior, W. Cunico, J. L. Wardell, S. M. S. V. Wardell, E. R. T. Tiekink, *Acta Cryst. E* **2011**, *67*, o2447.
[12] CrystalClear-SM Expert. User Manual. Rigaku/MSC Inc., Rigaku Corporation, The Woodlands, TX, **2011**.
[13] G. M. Sheldrick, *Acta Crystallogr. A* **2008**, *64*, 112.
[14] G. M. Sheldrick, *Acta Crystallogr. C* **2015**, *71*, 3.
[15] L. J. Farrugia, *J. Appl. Crystallogr.* **2012**, *45*, 849.
[16] A. L. Spek, *Acta Crystallogr. D* **2009**, *65*, 148.
[17] J. Gans, D. Shalloway, *J. Mol. Graph. Model.* **2001**, *19*, 557.
[18] DIAMOND, Visual Crystal Structure Information System, Version 3.1, CRYSTAL IMPACT, Postfach 1251, D-53002, **2006**.
[19] M. J. Frisch, G. W. Trucks, H. B. Schlegel, G. E. Scuseria, M. A. Robb, J. R. Cheeseman, G. Scalmani, V. Barone, B. Mennucci, G. A. Petersson, H. Nakatsuji, M. Caricato, X. Li, H. P. Hratchian, A. F. Izmaylov, J. Bloino, G. Zheng, J. L. Sonnenberg, M. Hada, M. Ehara, K. Toyota, R. Fukuda, J. Hasegawa, M. Ishida, T. Nakajima, Y. Honda, O. Kitao, H. Nakai, T. Vreven, J. A. Montgomery Jr., J. E. Peralta, F. Ogliaro, M. J. Bearpark, J. Heyd, E. N. Brothers, K. N. Kudin, V. N. Staroverov, R. Kobayashi, J. Normand, K. Raghavachari, A. P. Rendell, J. C. Burant, S. S. Iyengar, J. Tomasi, M. Cossi, N. Rega, N. J. Millam, M. Klene, J. E. Knox, J. B. Cross,

Q2: Please supply [illegible] number for ref. 2

V. Bakken, C. Adamo, J. Jaramillo, R. Gomperts, R. E. Stratmann, O. Yazyev, A. J. Austin, R. Cammi, C. Pomelli, J. W. Ochterski, R. L. Martin, K. Morokuma, V. G. Zakrzewski, G. A. Voth, P. Salvador, J. J. Dannenberg, S. Dapprich, A. D. Daniels, Ö. Farkas, J. B. Foresman, J. V. Ortiz, J. Cioslowski and D. J. Fox, Gaussian 09, Revision A.1, Gaussian, Inc., Wallingford, CT, USA, **2009**.

[20] O. A. Vydrov, G. E. Scuseria, *J. Chem. Phys*. **2006**, *125*, 234109.

[21] O. A. Vydrov, J. Heyd, A. V. Krukau, G. E. Scuseria, *J. Chem. Phys*. **2006**, *125*, 074106.

[22] A. D. Becke, E. R. Johnson, *J. Chem. Phys*. **2007**, *127*, 154108.

[23] A. Otero-de-la-Roza, E. R. Johnson, *J. Chem. Phys*. **2013**, 138, 204109.

[24] Freely available from https://github.com/aoterodelaroza/postg.

[25] S. K. Wolff, D. J. Grimwood, J. J. McKinnon, M. J. Turner, D. Jayatilaka, M. A. Spackman, Crystal Explorer (Version 3.1), University of Western Australia, **2012**.

[26] M. A. Spackman, J. J. McKinnon, D. Jayatilaka, *CrystEngComm* **2008**, *10*, 377.

[27] D. Jayatilaka, D. J. Grimwood, A. Lee, A. Lemay, A. J. Russel, C. Taylor, S. K. Wolff, C. Chenai, A. Whitton, TONTO – A System for Computational Chemistry, **2005**. Available at: http://hirshfeld-surface.net/.

[28] J. J. McKinnon, M. A. Spackman, A. S. Mitchell, *Acta Crystallogr. B* **2004**, *60*, 627.

[29] J. J. McKinnon, D. Jayatilaka, M. A. Spackman, *Chem Commun*. **2007**, 3814.

Supplemental Material: The online version of this article (DOI: 10.1515/zkri-2016-1990) offers supplementary material, available to authorized users.

Graphical Synopsis

Walcimar T. Vellasco Junior, Claudia R.B. Gomes, Thatyana R.A. Vasconcelos, James L. Wardell, A. Otero-de-la-Roza, Mukesh M. Jotani and Edward R.T. Tiekink

Crystallographic and computational study of *t*-butyl *N*-[3-hydroxy-1-phenyl-4-(pyridin-2-ylsulfanyl)butan-2-yl]carbamate and its pyrimidin-2-yl analogue

DOI 10.1515/zkri-2016-1990
Z. Kristallogr. 2016; x: xxx–xxx

Synopsis: Molecular packing influences the formation of intramolecular O-H…N hydrogen bonding.